Volume 245 · Issue 2 · October 2013   ISSN 0025-5564

ELSEVIER

Mathematical Biosciences
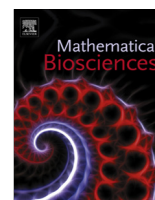
Review

Locating multiple tumors by moving shape analysis

CrossMark

Claudio Padra, Natalia Nieves Salva *

Centro Atómico Bariloche, Av. Bustillo 9500, 8400 Bariloche, Argentina

ARTICLE INFO

ABSTRACT

A methodology to determine the unknown shape of an embedded tumor is proposed. A functional that represents the mismatch between a measured experimental temperature profile, which may be obtained by infrared thermography at skin surface, and the solution of an appropriate boundary problem is defined. Using the Pennes's bioheat transfer equations, the temperature in a section of healthy tissue with a tumor region is modeled by a boundary problem. The functional is related to the shape of the tumor through the solution of the boundary problem, in such a way that finding the minimum of the functional form also means finding the unknown shape of the embedded tumor. The shape derivative of the functional is computed in each node of an approximation of the solution by the method of Finite Elements using similar methods considered by Pironneau [7]. The algorithm presented include an adaptive strategy to improve the error of the objective function. Numerical results with multiple connected tumors are considered to illustrate the potential of the proposed methodology.

© 2013 Elsevier Inc. All rights reserved.

1. Introduction

The modeling of heat transfer in organs has been studied by Pennes since 1948 [2,3]. He suggested that the rate of heat transfer between blood and tissue was proportional to the product of the volumetric perfusion rate and the difference between the arterial blood temperature and the local tissue temperature. Therefore the temperature of a tissue depends on the rate of blood perfusion, the metabolic activity and the heat conduction between the tissue and the environment. The physiological properties of a tumor may differ from a normal tissue, which produces an increase in the temperature of the skin [8–10]. By observing the superficial temperatures of the skin, the location and size of a tumoral tissue may be predicted.

Given the location and shape of a tumor, we can predict the temperature in all the domain. This problem is called the direct problem. The inverse problem consists of using the measurement of the skin temperature to infer the position of the tumor. While the direct problem is well-posed problem [11] (has a unique solution which depends continuously on the data), the inverse problem generally is not.

In [6] the boundary element method was used to locate tumor regions (which were assumed to be elliptical or ellipsoidal) and to find the unknown thermophysical parameters of these regions. In [4] unknown geometrical parameters of an embedded tumor were determined by computing a shape derivative, and solving the

differential and adjoint problem with a second order finite difference scheme. In [4] they assumed that the tumor was a spherical simply connected region. The goal of this work is to locate disconnected tumor regions with any shape. We developed an algorithm based on the reaction–diffusion equation, using the finite element method combined with a shape derivative which allows the tumor to change its shape in each iteration. The shape derivative is used to reduce the value of a objective function which measures the difference between the temperature data and its approximation, and is determined using an adjoint method similar to the one introduced in [7]. When a node of the triangulation is moved, it is important to control the error generated by the finite element solution. We developed a posteriori error estimation and use it for refinement and remeshing.

The following equation models the temperature of a skin tissue, $\phi(x)$, that has an embedded tumor region [6]:

$$-\sigma_i \Delta \phi(x) + k_i(\phi(x) - T_b) = q_i(x) \quad i = 1, 2 \quad for\ x \in \Omega, \tag{1}$$

where Ω represents the two dimensional skin tissue and $\bar{\omega}$ represents the embedded tumor. The sub index $i = 1, 2$ identifies the healthy tissue $\Omega - \bar{\omega}$ ($i = 1$) and the tumor region $\bar{\omega}$ ($i = 2$) (see Fig. 1), σ represents the thermal conductivity, k is the blood perfusion coefficient, q is the metabolic heat source and T_b is the constant blood temperature. Using the fact that the thermal conductivity, the blood perfusion and the metabolic activity are significantly higher in the tumor region than in normal tissue, we considered that all these coefficients are piecewise continuous. Defining $Q = q + kT_b$, we have the following simplified equation:

$$-\sigma_i \Delta \phi(x) + k_i \phi(x) = Q_i(x) \quad i = 1, 2. \tag{2}$$

* Corresponding author. Tel.: +54 294 444 5100.
 E-mail addresses: padra@cab.cnea.gov.ar (C. Padra), natalia.salva@yahoo.com.ar (N.N. Salva).
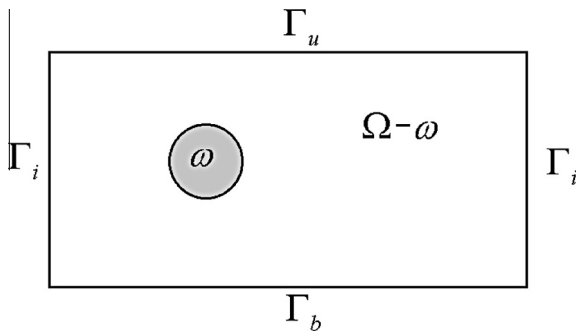
Fig. 1. Two dimensional domain. $\Omega-\omega$ healthy tissue and ω tumor region.

If we define $\phi_1 = \phi|_{\Omega-\bar{\omega}}$ and $\phi_2 = \phi|_{\omega}$, we have the following boundary conditions:

$$\begin{cases} (i) & \phi_1 = \phi_2 & \text{on } \partial\omega, \\ (ii) & -\sigma_1 \frac{\partial \phi_1}{\partial n} = -\sigma_2 \frac{\partial \phi_2}{\partial n} & \text{on } \partial\omega, \\ (iii) & -\sigma_1 \frac{\partial \phi_1}{\partial n} = \alpha(\phi_1 - T_a) & \text{on } \Gamma_u, \\ (iv) & -\sigma_1 \frac{\partial \phi_1}{\partial n} = 0 & \text{on } \Gamma_i, \\ (v) & \phi_1 = T_b & \text{on } \Gamma_b, \end{cases} \quad (3)$$

where α is the heat transfer coefficient, T_a is the ambient temperature, and n is the outward pointing unit normal. Conditions $(3)(i,ii)$ represent the ideal thermal contact between healthy tissue and tumor. A constant core temperature T_b is assumed $(3)(v)$, and a no-flux condition in the lateral boundaries $(3)(iv)$. The convective condition $(3)(iii)$ represents the interchange of temperature between the body and the environment.

The physiological properties of a tumor may produce an increase in the temperature of the skin [8–10], and by observing the superficial temperatures of the skin, the location and size of a tumoral tissue may be predicted. Let ϕ_o be the temperature measured on the boundary Γ_u, which represents the superficial skin, and ϕ_ω the solution of the problem (2) and (3), which depends on the location and shape of ω. The objective function is defined by:

$$E(\omega, \phi_\omega) = \int_{\Gamma_u} | \phi_\omega - \phi_o|^2 d\Gamma. \quad (4)$$

The goal is to find $\omega^* \subset \Omega$ such that the respective solution ϕ_* of the problem (2) and (3) verifies: $E(\omega^*, \phi_*) = 0$, which implies that $\phi_* = \phi_o$ in Γ_u. An equivalent way of defining the problem is the following:

$(P)\begin{cases} \text{Given the following thermophysical constants}: \sigma, k, q, T_b, T_a, \alpha \text{ and the temperature } \phi_o \\ \text{at the boundary } \Gamma_u, \text{ find } \omega^* \subset \Omega, \text{such that the respective solution } \phi_* \text{of the problem} \\ (2)-(3) \text{produces the minimum of the functional } E, \text{i.e.}: E(\omega^*, \phi_*) = \min_{\omega \subset \Omega} E(\omega, \phi_\omega). \end{cases}$

2. Variational formulation and discretization of the problem (2) and (3)

The variational formulation of the problem (2) and (3), is the following [4]:

$$\begin{cases} \text{Find } \phi \in H^1(\Omega) \text{ such that} \\ a(\phi, v) = L(v), \quad \forall v \in V(\Omega) \\ \phi = T_b \quad \text{on } \Gamma_b \end{cases} \quad (5)$$

where a, L and $V(\Omega)$ are defined as follows:

$$a(\phi, v) = \int_\Omega (\sigma \nabla \phi \nabla v + k\phi v)dx + \alpha \int_{\Gamma_u} \phi v d\Gamma, \quad (6)$$

$$L(v) = \int_\Omega Q v dx + \alpha T_a \int_{\Gamma_u} v d\Gamma, \quad (7)$$

$$H^1(\Omega) = \{v \in L^2(\Omega)/\|v\|_{H^1(\Omega)} < \infty\}, \quad \|v\|_{H^1(\Omega)} = \left(\|v\|^2_{L^2(\Omega)} + \|\nabla v\|^2_{L^2(\Omega)}\right)^{1/2}, \quad (8)$$

$$V(\Omega) = \{v \in H^1(\Omega) : v = 0 \text{ on } \Gamma_b\}. \quad (9)$$

We recall that $\|\nabla v\|_{L^2(\Omega)}$ is equivalent to $\|v\|_{H^1(\Omega)}$ in the space $V(\Omega)$.

Let $\{\mathcal{T}_h\}$ be a family of triangulations of Ω such that any two triangles in $\mathcal{T}_h$ have at most a vertex or an edge. For the triangulation $\mathcal{T}_h$, let M be the number of triangles, N the number of nodes, and G the set of index of the nodes which are on the Dirichlet boundary Γ_b. Let h_T stand for the diameter of the triangle $T \in \mathcal{T}_h$, and h the maximum of $h_T, T \in \mathcal{T}_h$. We assume that the family of triangulations $\{\mathcal{T}_h\}$ satisfies the minimum angles condition and, consequently, there exists a constant $\Theta > 0$ such that $h_T/d_T < \Theta$, where d_T is the diameter of the largest circle contained in T. Throughout this work we will denote by c a generic positive constant, not necessarily the same at each occurrence, which may depend on the mesh only through the parameter Θ.

We define the following finite element spaces:

$$V_h^1(\Omega) = \{w_h \in H_h^1(\Omega) : w_h|_{\Gamma_b} = 0\} \quad (10)$$

where

$$H_h^1(\Omega) = \{w_h \in C^o(\Omega) : w_h|_{T_k} \in P^1(T_k) \quad \forall T_k \in \mathcal{T}_h\} \quad (11)$$

$P^1(T)$the space of the polynomials of degree less or equal to 1 in T $\quad (12)$

We use $H_h^1(\Omega)$ and $V_h^1(\Omega)$ to approximate $H^1(\Omega)$ and $V(\Omega)$, respectively. Then ϕ can be approximated by a function $\phi_h \in H_h^1(\Omega)$ the solution of the problem:

$$\begin{cases} \text{Find } \phi_h \in H_h^1(\Omega) \text{ such that} \\ a(\phi_h, w_h) = L(w_h), \quad \forall w_h \in V_h^1(\Omega) \\ \phi_h = T_b \quad \text{on } \Gamma_b \end{cases} \quad (13)$$

The problem (13) can be solved by finding a solution of a linear matrix system:

$$A\phi_{\mathbf{h}} = F, \quad (14)$$

where

$$A_{ij} = a(\eta_i, \eta_j), \quad F_i = L(\eta_i), \quad (15)$$

$$\phi_{\mathbf{h}} = (\phi_1, \phi_2, \ldots, \phi_N)^T, \quad \phi_h = \sum_{i \notin G} \phi_i \eta_i + \sum_{i \in G} T_b \eta_i, \quad (16)$$

$\{\eta_j\}_{j=1,\ldots,N}$ is a base of $H_h^1(\Omega)$ and $\{q_i\}_{i \in G}$ are the nodes in Γ_b. (17)

It is easy to show that the matrix A is positively defined and symmetric, and therefore a unique solution exists. If $\{q_i\}_{i=1,\ldots,N}$ are the vertex of the triangles of $\mathcal{T}_h$, the base $\{\eta_j\}_{j=1,\ldots,N}$ of $H_h^1(\Omega)$ is uniquely determined by:

$$\eta_i(q_j) = \delta_{ij} \quad \forall i, j = 1, \ldots, N. \quad (18)$$

Then, (4) can be approximated by:

$$E(\omega_h, \phi_h) = \sum_{l \in \Gamma_u} \int_l | \phi_h - \phi_o|^2 d\Gamma. \quad (19)$$

We define the following Approximated Problem of (P):

$(A.P.)\begin{cases} \text{Given the following thermophysical constants}: \sigma, k, q, T_b, T_a, \alpha \text{ and the temperature} \\ \phi_o \text{ in the boundary } \Gamma_u, \text{ find } \omega_h^* \subset \Omega, \text{such that the respective solution } \phi_h^* \text{of the} \\ \text{problem (15) gives the minimum of the functional } E, \text{i.e.}: E(\omega_h^*, \phi_h^*) = \min_{\Omega = \cup T_k} E(\omega_h, \phi_h) \end{cases}$

2.1. Adjoint problem and the shape derivative

The adjoint problem of the problem (5) is to find $p \in H_h^1(\Omega)/p|_{\Gamma_b} = 0$, where p is the solution of the following differential problem:

$$
\begin{cases}
(i) & -\sigma \Delta p + kp = 0 & \text{on } \Omega, \\
(ii) & -\sigma \frac{\partial p}{\partial n} = \alpha(p - \frac{2}{\alpha}(\phi_h - \phi_o)) & \text{on } \Gamma_u, \\
(iii) & \frac{\partial p}{\partial n} = 0 & \text{on } \Gamma_i, \\
(iv) & p = 0 & \text{on } \Gamma_b.
\end{cases}
\tag{20}
$$

The variational formulation of (20) can be approximated by a function $p_h \in V_h^1(\Omega)$ such that:

$$
a(p_h, w_h) = 2 \int_{\Gamma_u} (\phi_h - \phi_o) w_h d\Gamma, \quad \forall w_h \in V_h^1(\Omega).
\tag{21}
$$

This last problem is equivalent to a linear matrix problem:

$$
A\mathbf{p_h} = \widetilde{F},
\tag{22}
$$

where

$$
\widetilde{F}_i = 2 \int_{\Gamma_u} (\phi_h - \phi_o) \eta_i d\Gamma,
\tag{23}
$$

$$
\mathbf{p_h} = (p_1, p_2, \ldots, p_N)^T, \quad p_h = \sum_{i \notin G} p_i \eta_i.
\tag{24}
$$

The matrix A is defined by (15) and therefore a unique solution exists.

3. Shape derivative

Using similar techniques to the ones developed by Pironneau [7], one can define a derivative of the objective function E with respect to each node of the triangulation. This derivative shows in which direction we should move q_k to have a maximum increase of E, thus if we move it in the opposite direction, we would have a maximum decrease of the value of E [1].

Theorem 1. If E is given by (19), ϕ_h is the solution of (13), and p_h is the solution of (21), then

$$
\frac{\partial E}{\partial q_k^l} = \int_\Omega \frac{\partial p_h}{\partial x_l}(q_k)(\sigma \nabla \eta_k \nabla \phi_h + \eta_k(k\phi_h - Q))dx
$$
$$
- \int_\Omega \frac{\partial}{\partial x_l}[\eta_k(p_h(k\phi_h - Q) + \sigma \nabla \phi_h \nabla p_h)]dx,
\tag{25}
$$

where $q_k = (q_k^1, q_k^2)$ are the nodes of the triangulation $\mathcal{T}_h, l = 1, 2$ represents the coordinates and $\{\eta_j\}_{j=1,\ldots,N}$ is the base of $H_h^1(\Omega)$.

Proof 1. See [1].

4. A posteriori error estimations

When the nodes of the mesh are moved, sometimes the triangles can degenerate, having an area close to zero. This is the reason for the remeshing in each iteration. After some iterations, the size of the triangles of the mesh must be reduce to improve the values of the temperature in the boundary Γ_u, therefore a refinement is needed. The problem is where to refine. In this section we introduce estimators for the temperature error $\phi - \phi_h$ and the adjoint error $p - p_h$. Using this estimators we can find a bound for the objective function.

4.1. Estimator of the objective function

Theorem 2. Let ϕ_ω and p_ω be the solutions of (5) and (20), respectively, and ϕ_h and p_h the solutions of their approximated problems in the spaces $H_h^1(\Omega)$ and $V_h^1(\Omega)$, respectively. Then for all $\gamma > 0$:

$$
| E(\omega, \phi_\omega) - E(\omega_h, \phi_h) | \leqslant c \left(\frac{\gamma}{2} \|\phi_\omega - \phi_h\|_{H^1(\Omega)}^2 + \frac{1}{2\gamma} \|p_\omega - p_h\|_{H^1(\Omega)}^2 \right)
$$
$$
+ \text{h.o.t.},
$$

where h.o.t. represents higher order terms.

Proof 2. Is easy to verify that:

$$
E(\omega, \phi_\omega) - E(\omega_h, \phi_h) = 2 \int_{\Gamma_u} (\phi_h - \phi_o)(\phi_\omega - \phi_h)d\Gamma
$$
$$
+ \int_{\Gamma_u} (\phi_\omega - \phi_h)^2 d\Gamma.
\tag{26}
$$

The first term of (26) is bounded by:

$$
\left| 2 \int_{\Gamma_u} (\phi_h - \phi_o)(\phi_\omega - \phi_h)d\Gamma \right| \leqslant a(\phi_\omega - \phi_h, p_\omega)
$$
$$
= a(\phi_\omega - \phi_h, p_\omega - p_h)
$$

$$
\leqslant c\|\phi_\omega - \phi_h\|_{H^1(\Omega)}\|p_\omega - p_h\|_{H^1(\Omega)}
$$
$$
\leqslant c \left(\frac{\gamma}{2} \|\phi_\omega - \phi_h\|_{H^1(\Omega)}^2 + \frac{1}{2\gamma} \|p_\omega - p_h\|_{H^1(\Omega)}^2 \right), \quad \forall \gamma > 0.
$$

The second term of (26) is a higher order term which can be neglected. In fact,

$$
\int_{\Gamma_u} (\phi_\omega - \phi_h)^2 d\Gamma \leqslant ch\|\nabla \phi_\omega - \nabla \phi_h\|_{L^2(\Omega)}^2 \leqslant ch\|\phi_\omega - \phi_h\|_{H^1(\Omega)}^2.
$$

By the previous theorem, for the estimation of the error of the objective function it is necessary to estimate the errors of the temperature and adjoint temperature.

4.2. Temperature estimator

We define the *local indicator* η_T in each triangle T of the triangulation $\mathcal{T}_h$ for problem (5) by:

$$
\eta_T = \left(h_T^2 \int_T | R_T |^2 dx + \sum_{l \subset \partial T} h_l \int_l | J_l |^2 d\Gamma \right)^{1/2},
\tag{27}
$$

where

$$
h_l = |l|, \quad h_T = \max_{l \text{ side of } T} h_l,
\tag{28}
$$
$$
R_T = Q + \sigma \Delta \phi_h - k\phi_h = Q - k\phi_h,
\tag{29}
$$

$$
J_l = \begin{cases}
-\sigma_1 \frac{\partial \phi_h}{\partial n} & \text{if } l \subset \Gamma_i, \\
0 & \text{if } l \subset \Gamma_b, \\
-\sigma_1 \frac{\partial \phi_h}{\partial n} - \alpha(\phi_h - T_a) & \text{if } l \subset \Gamma_u, \\
-\frac{1}{2}(\sigma^+ \nabla \phi_h^+ - \sigma^- \nabla \phi_h^-) \cdot n & \text{if } l \subset \mathcal{E}_I,
\end{cases}
\tag{30}
$$

l is a side of T and $\mathcal{E}_l$ is the set of interior sides.

We remark that J_l represents the residual in each side l of the triangulation and R_T represents the volumetric residual en each triangle T.

The *global estimator* η is then defined as:

$$\eta = \left(\sum_{T \in \mathcal{T}_h} \eta_T^2 \right)^{1/2}. \tag{31}$$

Lemma 1. *Let ϕ be the solution of* (5) *and let ϕ_h be the solution of* (13). *If $e = \phi - \phi_h \in V(\Omega)$ is the error, the Error Equation for this problem is:*

$$\int_\Omega \sigma \nabla e \nabla v + k e v \, dx + \alpha \int_{\Gamma_u} e v \, d\Gamma = \sum_{T \in \mathcal{T}_h} \int_T R_T(v - v_h) dx$$

$$+ \sum_{l \subset \partial T} \int_l J_l(v - v_h) d\Gamma \quad \forall v \in V(\Omega), \ \forall v_h \in V_h^1(\Omega), \tag{32}$$

where J_l and R_T are given by (30) *and* (29), *respectively.*

Proof 3. Observe that:

$$\int_\Omega \sigma \nabla e \nabla v_h + k e v_h \, dx + \alpha \int_{\Gamma_u} e v_h \, d\Gamma = 0 \quad \forall v_h \in V_h^1(\Omega). \tag{33}$$

Using (5) and (33):

$$\int_\Omega \sigma \nabla e \nabla v + k e v \, dx + \alpha \int_{\Gamma_u} e v \, d\Gamma = = \sum_{T \in \mathcal{T}_h} \left(\int_T (Q - k\phi_h)(v - v_h) \right.$$
$$- \sigma \nabla \phi_h \nabla(v - v_h) dx)$$
$$\left. - \int_{\Gamma_u} \alpha(\phi_h - T_a)(v - v_h) d\Gamma. \right. \tag{34}$$

Integrating by parts in each triangle T, we obtain the Error Equation.

Theorem 3. *Let ϕ and ϕ_h be the solution of* (5) *and* (13), *respectively. Then there exists a constant $c > 0$ such that:*

$$\|\phi - \phi_h\|_{H^1(\Omega)} \leqslant c\eta. \tag{35}$$

Proof 4. We denote $e^I \in V_h^1(\Omega)$ the Clément interpolation which is defined in [5]. The following error estimate, which can be easily proved by using the results from this reference, hold for this interpolation:

$$\left(\sum_{T \in \mathcal{T}_h} (\|e - e^I\|_{L^2(T)}^2 h_T^{-2} + \sum_{l \subset \partial T} \|e - e^I\|_{L^2(l)}^2 h_l^{-1}) \right)^{1/2} \leqslant c \|\nabla e\|_{L^2(\Omega)}. \tag{36}$$

Taking $v = e$ and $v_h = e^I$ in the Error Equation of Lemma 1 and applying the Cauchy–Schwartz inequation:

$$\int_\Omega \sigma \mid \nabla e \mid^2 + k \mid e \mid^2 dx + \alpha \int_{\Gamma_u} \mid e \mid^2 d\Gamma$$

$$\leqslant \left(\sum_{T \in \mathcal{T}_h} \left(h_T^2 \|R_T\|_{L^2(T)}^2 + + \sum_{l \subset \partial T} h_l \|J_l\|_{L^2(l)}^2 \right) \right)^{1/2}$$

$$\cdot \left(\sum_{T \in \mathcal{T}_h} \left(\|e - e^I\|_{L^2(T)}^2 h_T^{-2} + \sum_{l \subset \partial T} \|e - e^I\|_{L^2(l)}^2 h_l^{-1} \right) \right)^{1/2}. \tag{37}$$

From (36) and (37) we obtain the following:

$$\|e\|_{H^1(\Omega)} \leqslant c \left(\sum_{T \in \mathcal{T}_h} \eta_T^2 \right)^{1/2}. \tag{38}$$

Theorem 4. *Let ϕ and ϕ_h be the solution of* (5) *and* (13), *respectively. Then there exists a constant $c > 0$ such that $\forall T \in \mathcal{T}_h$:*

$$\eta_T \leqslant c \|\phi - \phi_h\|_{H^1(T^*)}, \tag{39}$$

where $T^* = \cup\{\widetilde{T} \in \mathcal{T}_h / \widetilde{T} \cap T \neq \emptyset, \widetilde{T} \cap T \neq \{P\}\}$, i.e., T^* is the union of all the triangles that share a side with T.

Proof 5. If the vertex of T are $\{z_1, z_2, z_3\}$, then we define the *ith barycentric coordinate* $\lambda_i(x, y) \in P^1(T)/\lambda_i(z_j) = \delta_{ij}$. Let $b_T = 27\lambda_1\lambda_2\lambda_3$ be the *cubic bubble of T*. Replacing $v = R_T b_T$ and $v_h = 0$ in the Error Equation, and observing that b_T is zero in every side of T, we have that:

$$\int_T \sigma \nabla e \nabla R_T b_T + k R_T b_T e \, dx + \alpha \int_{\Gamma_u \cap T} e R_T b_T d\Gamma = \int_T R_T^2 b_T dx. \tag{40}$$

Taking into account that all the norms are equivalent in finite dimensional spaces ($P^4(T)$), there exists a constant $c > 0$ such that:

$$\int_T v^2 dx \leqslant c \int_T v^2 b_T dx. \tag{41}$$

On the other hand, by the Inverse Inequality, there exists a constant $c > 0$, such that:

$$\|\nabla v\|_{L^2(T)} \leqslant \frac{c}{h_T} \|v\|_{L^2(T)}. \tag{42}$$

Using the Cauchy–Schwarz Inequality, (41) and (42) and the fact that the cubic bubble is less than 1, we have that:

$$\|R_T\|_{L^2(T)}^2 \leqslant \frac{c}{h_T} \|e\|_{H^1(T)} \|R_T\|_{L^2(T)} \tag{43}$$

and dividing by $\|R_T\|_{L^2(T)}$:

$$\left(h_T^2 \int_T R_T^2 dx \right)^{1/2} \leqslant c \|e\|_{H^1(T)}. \tag{44}$$

Let l be a side of the triangle T. If l is in the interior of the domain Ω, then $l = T \cap \widetilde{T}$ for some $\widetilde{T} \in T^*$. In this case we replace $v = J_l \psi_l$ and $v_h = 0$ in the Error Equation, with $\psi_l = 4\lambda_1\lambda_2$ in T and $\widetilde{T}$ (if z_1 and z_2 are the vertex of l). If l is over the boundary, we replace $v = J_l \psi_l$ and $v_h = 0$ in the Error Equation, with $\psi_l = 4\lambda_1\lambda_2$ in T. In the case where l is interior, we have:

$$\int_{T \cup \widetilde{T}} \sigma \nabla e \nabla J_l \psi_l + k J_l \psi_l e \, dx = \int_{T \cup \widetilde{T}} R_T J_l \psi_l dx + \int_l J_l^2 \psi_l d\Gamma. \tag{45}$$

Observing that J_l is constant in l, that $\psi_l \leqslant 1$ and using (42) and (44), we have that:

$$\frac{2}{3} h J_l^2 = \int_l J_l^2 \psi_l d\Gamma \leqslant c \mid J_l \mid \|e\|_{H^1(T \cup \widetilde{T})}. \tag{46}$$

Rearranging the terms, we obtain that for each $\widetilde{T} \in T^*$:

$$\left(h_l \int_l J_l^2 d\Gamma \right)^{1/2} = h_l \mid J_l \mid \leqslant c \|e\|_{H^1(T \cup \widetilde{T})}. \tag{47}$$

Likewise, if l belongs to the boundary $\partial\Omega - \Gamma_u$, we can obtain a similar inequality. If l belongs to Γ_u, J_l is lineal, and in this case the Error Equation can be bounded in the following way:

$$\int_l J_l^2 \psi_l d\Gamma \leqslant \frac{c}{h_T} \|e\|_{H^1(T)} \|J_l \psi_l\|_{L^2(T)}. \tag{48}$$

The equivalence of the norms of $L^\infty(l)$ and $L^2(l)$ in the space of the polynomials of degree less or equal than 2 implies that:

$$\|J_l \psi_l\|_{L^2(T)} \leqslant h_T \max_l |J_l| \leqslant c h_T^{1/2} \|J_l \psi_l\|_{L^2(l)}. \tag{49}$$

Then, by the previous property and (48) we have that

$$\left(h_l \int_l J_l^2 \psi_l d\Gamma\right)^{1/2} \leqslant c\|e\|_{H^1(T)}. \tag{50}$$

Finally, from (44) and (47), (39) is obtained.

4.3. Adjoint estimator

We define the *local adjoint indicator* μ_T in each triangle T of the triangulation $\mathcal{T}_h$, for the problem (21), in the following way:

$$\mu_T = \left(h_T^2 \int_T |R_T^a|^2 dx + \sum_{l \subset \partial T} h_l \int_l |J_l^a|^2 d\Gamma\right)^{1/2}, \tag{51}$$

where

$$h_l = \|l\|, \quad h_T = \max_{l \text{ a side of } T} h_l, \tag{52}$$

$$J_l^a = \begin{cases} -\sigma_1 \frac{\partial p_h}{\partial n} & \text{if } l \subset \Gamma_i, \\ 0 & \text{if } l \subset \Gamma_b, \\ -\sigma_1 \frac{\partial p_h}{\partial n} - \alpha p_h + 2(\phi_h - \phi_o) & \text{if } l \subset \Gamma_u, \\ -\frac{1}{2}(\sigma^+ \nabla p_h^+ - \sigma^- \nabla p_h^-) \cdot n & \text{if } l \subset \mathcal{E}_I, \end{cases} \tag{53}$$

$$R_T^a = \sigma \Delta p_h - k p_h = -k p_h. \tag{54}$$

The *global adjoint estimator* μ is defined by:

$$\mu = \left(\sum_{T \in \mathcal{T}_h} \mu_T^2\right)^{1/2}. \tag{55}$$

Lemma 2. *Let p and p_h be the solutions of (20) and (21), respectively. If $e^a = p - p_h \in V(\Omega)$ is the adjoint error, then the Error Equation for this problem is the following:*

$$\int_\Omega \sigma \nabla e \nabla v + k e v dx + \alpha \int_{\Gamma_u} e v d\Gamma$$
$$= \sum_{T \in \mathcal{T}_h} \int_T R_T^a(v - v_h) dx + \sum_{l \subset \partial T} \int_l J_l^a(v - v_h) d\Gamma \quad \forall v$$
$$\in V(\Omega), \ \forall v_h \in V_h^1(\Omega), \tag{56}$$

where J_l^a and R_T^a are given by (53) and (54), respectively.

Theorem 5. *Let p and p_h be the solutions of (20) and (21), respectively. Then there exists a constant $C > 0$ such that:*

$$\|e^a\|_{H^1(\Omega)} \leqslant c\mu. \tag{57}$$

Proof 6. Similar to Theorem 3.

Theorem 6. *Let p and p_h be the solutions of (20) and (21), respectively. Then there exists a constant $c > 0$ such that $\forall T \in \mathcal{T}_h$:*

$$\mu_T \leqslant c\|e^a\|_{H^1(T^*)}. \tag{58}$$

where T^* is given by Theorem 4.

Proof 7. Similar to Theorem 4.

We define the *local objective function indicator* ξ_T in each triangle T of the triangulation $\mathcal{T}_h$, in the following way:

$$\xi_T = \left(\frac{\gamma}{2} h_T^2 + \frac{1}{2\gamma} \mu_T^2\right)^{1/2}, \tag{59}$$

where $\gamma = \sqrt{\max_j\{\eta_j\}/\max_j\{\eta_j^a\}}$. The choice of this γ shows that $\max\{\frac{\gamma}{2}\mu_T^2\} = \max\{\frac{1}{2\gamma}\eta_T^2\}$, which implicates that triangles with high η_T will we refined in the same way as the ones with high μ_T. The *global objective function estimator* ξ is then defined as:

$$\xi = \left(\sum_{T \in \mathcal{T}_h} \xi_T^2\right)^{1/2}. \tag{60}$$

Corolary 1. *Let ϕ_ω and p_ω be the solutions of (5) and (20), respectively, and ϕ_h and p_h the solutions of their approximated problems in the spaces $H_h^1(\Omega)$ and $V_h^1(\Omega)$, respectively. Then:*

$$|E(\omega, \phi_\omega) - E(\omega_h, \phi_h)|^{1/2} \leqslant c\xi + h.o.t.$$

where h.o.t represents higher order terms.

5. Numerical results

In this section we present different numerical simulations, carried out on a domain of 3 cm depth and 9 cm length. In the first example, the data was generated by a single connected tumor region, which shows how the shape derivative works. In the second place, the data was generated with two connected tumor regions, but the initial tumor for the algorithm was a single tumor region. In all of these we considered the following thermophysical constants [4]:

$$\sigma_1 = 0.5 \, [W/mK], \quad k_1 = 1998.1 \, [W/m^3K], \quad Q_1 = 74349.7 \, [W/m^3],$$
$$\sigma_2 = 0.75 \, [W/mK], \quad k_2 = 7992.4 \, [W/m^3K], \quad Q_2 = 299918.8 \, [W/m^3],$$
$$T_b = 37°C, \quad T_a = 25°C, \quad \alpha = 10[W/m^2K]. \tag{61}$$

We present two algorithms, one of which only moves the boundary of the tumor, and another that also minimizes the error of the objective function.

5.1. Algorithm without refinement

0. Choose an initial triangulation given by the nodes $\{q_k^{(0,0)}\}_{k=1,...,N_o}$. Choose R (number of iterations) and $\widehat{M}$ (number of movements in each iteration).

For $r = 0, \ldots, R$:
1. For $m = 0, \ldots, \widehat{M}$:
   (a) Calculate $\phi_h^{(r,m)}, p_h^{(r,m)}$ using (13) and (21).
   (b) Calculate the derivative $g_k^{(r,m)} = (g_{k_1}^{(r,m)}, g_{k_2}^{(r,m)})$ in each node $q_k^{(r,m)}$ using (25), for $k = 1, \ldots, N_r$.
   (c) Let $q_k^{(r,m)}(\rho) = q_k^{(r,m)} - \rho \cdot g_k^r$.
   (d) Compute $\rho_{max}^{(r,m)}$ the maximum allowable ρ such that it minimizes $E(q_k^{(r,m)}(\rho))$ (using Algorithm 3, page 51 of [7]).
   (e) Set $q_k^{(r,m+1)} = q_k^{(r,m)} - \rho_{max}^{(r,m)} g_k^r$.
2. Keeping only the nodes on $\partial\omega$, remesh Ω using the program **Gmsh©**, and save this triangulation as $\{q_k^{(r+1,0)}\}_{k=1,...,N_{r+1}}$.

5.2. Algorithm with refinement

For remeshing the domain we used the program **Gmsh©**, which has 2 inputs, one file with extension **geo** and another with extension **pos**. The file **geo** has the information of the domain, defining the boundaries Γ_u, Γ_i and Γ_b, and the segments that approximate the boundary of the tumor $\partial\omega$. To indicate the size of the triangles of the mesh, we use the file **pos**, which consists on another mesh, where each nodes has assigned a number that indicates the approximate size of the edges of the new triangles nearby. In the file **geo** the data of the last iteration are saved, in particular the boundary $\partial\omega$ and the new segments added by the last remeshing.

For the refinement of the mesh, we do the following:

1. Calculate the error estimators η_j and η_j^a en each triangle $\{T_j\}_{j=1\ldots M}$ of the mesh.
2. Define $\gamma = \sqrt{\max_j\{\eta_j\}/\max_j\{\eta_j^a\}}$.
3. Define a new matrix with the triangles's barycenter: $\tilde{q}_j, \forall j = 1 \ldots M$.
4. Establish a refinement bound, in this case $estmax = 0.5 \max_{j=1\ldots M}\{\frac{\gamma}{2}\eta_j^a + \frac{1}{2\gamma}\eta_j\}$.
5. Create the vector $bm \in \mathbb{R}^M$, such that:

$$bm(j) = \begin{cases} bm(j) = 0.25 \max_{l\text{size of}T_j}\{|\,l\,|\} & \text{if } \frac{\gamma}{2}\eta_j^a + \frac{1}{2\gamma}\eta_j > estmax \\ bm(j) = \frac{1}{3} \sum_{l\text{size of}T_j}\{|\,l\,|\} & \text{if not} \end{cases}$$

6. Assign $bmmax(k) = \min_{q_k \in T_{j_k}}\{bm(j_k)\}$ to each node q_k.
7. Assign $bm(j)$ to the nodes $\tilde{q}_j$ whose triangles have local estimator $\eta_j > estmax$.
8. Make a new triangulation with the nodes $\{q_k\}_{k=1,\ldots,N}$ and the ones chosen in the previous item. This triangulation with the assigned values is the background mesh.

The final algorithm is the following:

0. Choose an initial triangulation given by the nodes $\{q_k^{(0,0)}\}_{k=1,\ldots,N_o}$. Choose R (number of iterations), $\widehat{M}$(number of movements in each iteration), and I (the number of refinement in each iteration).
   For $r = 0,\ldots,R$:

1. For $m = 0,\ldots,\widehat{M}$:
   (a) Calculate $\phi_h^{(r,m)}, p_h^{(r,m)}$ using (13) and (21).
   (b) Calculate the derivative $g_k^{(r,m)} = (g_{k_1}^{(r,m)}, g_{k_2}^{(r,m)})$ in each node $q_k^{(r,m)}$ using (25), for $k = 1,\ldots,N_r$.
   (c) Let $q_k^{(r,m)}(\rho) = q_k^{(r,m)} - \rho . g_k^r$.
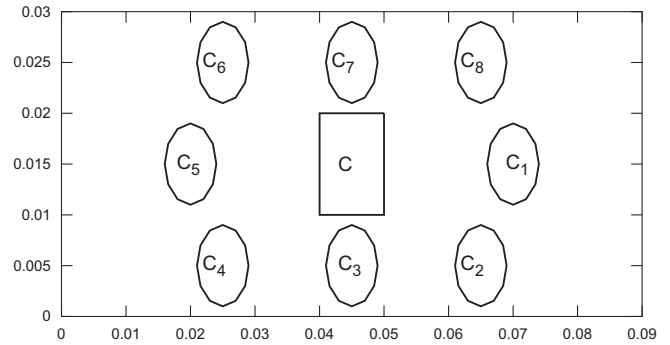

Fig. 2. Tumoral domains for the simulations.

   (d) Compute $\rho_{max}^{(r,m)}$ the maximum allowable ρ such that it minimizes $E(q_k^{(r,m)}(\rho))$ (using Algorithm 3, page 51 of [7]).
   (e) Set $q_k^{(r,m+1)} = q_k^{(r,m)} - \rho_{max}^{(r,m)}g_k^r$.
2. Keep only the nodes on $\partial\omega$, and remesh Ω.
3. For $i = 1,\ldots,I$
   (a) Calculate $\eta_{T_j}^2 = \frac{\gamma}{2}\eta_j^{a2} + \frac{1}{2\gamma}\eta_j^2$, assign $bm(j)$ to each triangle T_j.
   (b) With this values create a new background mesh.
   (c) Remesh Ω using **Gmsh©**, using the background mesh of the previous item.
4. Save the last triangulation as $\{q_k^{(r+1,0)}\}_{k=1,\ldots,N_{r+1}}$.

5.3. Simulations with a connected tumor region

To generate the "data" we supposed that the tumor region was the square C (see Fig. 2). We made simulations for eight different cases, replacing ω_o for the circles C_i for $i = 1..8$. We could observe that the results were symmetric to the vertical axis $x = 0.045$, for example the cases for $i = 8$ and $i = 5$ approached the region C in a similar way. Therefore we will just show the cases for $i = 1, 2, 3, 7, 8$. In all these cases we made 120 iterations, where for the first 60 we used the algorithm without refinement (5.1), and for the last 60 we used the other algorithm (5.2), taking $I = 4$ up to iteration 100, and $I = 5$ after that. This is due to the fact that as the temperature at the boundary Γ_u approaches to the data the mesh needs to be refined in that boundary to improve the values of the objective function.

5.3.1. $\omega_o = C_2$

In this case the domain ω_{32} divided in two sub-domains at the iteration N° 32. One sub-domain stays near ω_o while the other continuous to approximate to C. In the Fig. 3(a) we observe how the objective function decreases while the number of iterations increases. The oscillations are due to the remeshing, while the value
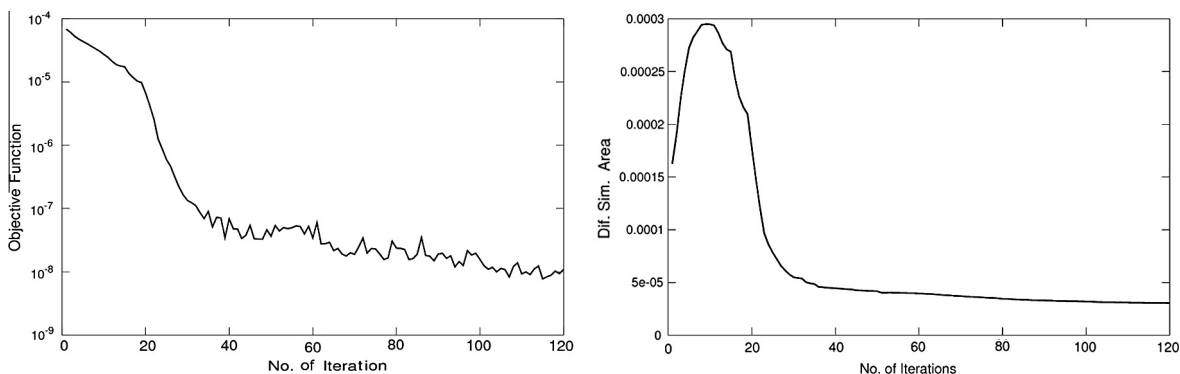

Fig. 3. a) Value of the target function (in logarithm scale) for each iteration, for the case of $i = 2$. b) Value of the area of the symmetric difference between C and ω_i for each $i = 1\ldots120$.
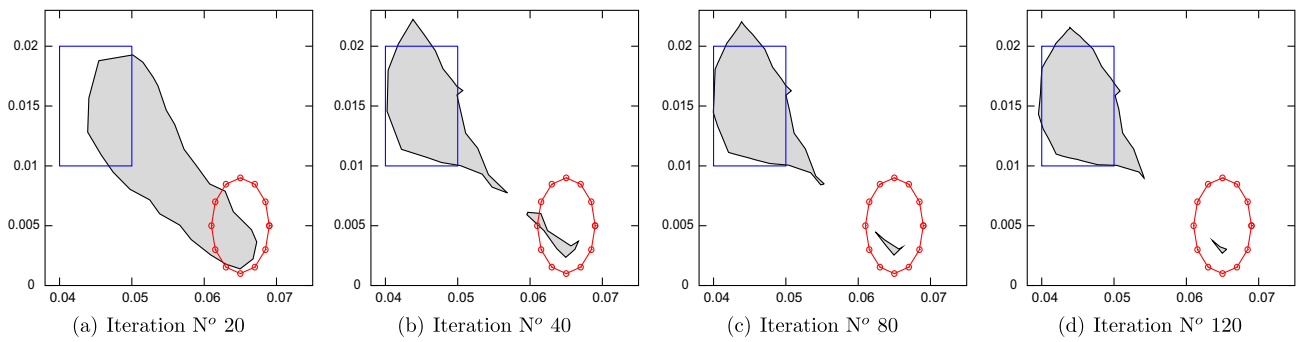
(a) Iteration N° 20 (b) Iteration N° 40 (c) Iteration N° 80 (d) Iteration N° 120

Fig. 4. Results of the movement for C_2.

Table 1
References of the movement.

— Objective Domain
-o-o- Initial Position
▦ Position of the i-th iteration

Fig. 6. Value of the target functino (in logarithm scale) for disconnected tumors.

of the objective functions decreases in the first mesh. When we re-mesh this value changes. In the Fig. 3(b) we plot the area of the symmetric difference between C and ω_i for each $i = 1 \ldots 120$. This area measures how good the approximation geometrically is. We observe that from the iteration N° 11 the area starts to decrease, because at this point the intersection between the two sets is not empty space. In the Fig. 4 we can observe the movement of the boundary tumor, and in Table 1 its references.

5.3.2. Cases for $i = 1, 3, 7, 8$

In Fig. 5 we observe the final iteration for each case, and in Table 1 its references. The final values of the objective function are: $7.144 \times 10^{-8}, 2.023 \times 10^{-7}, 2.172 \times 10^{-7}$ and 1.182×10^{-7} for C_1, C_3, C_7 and C_8, respectively. For $i = 3$ we observe that the domain stretches vertically, and the bottom part of the boundary does not move. Firstly, it stretches horizontally, and while it starts to stretch vertically, its width decreases. For $i = 7$ it has the opposite behavior, firstly it shrinks and then moves toward C. In the last iterations the locations does not change, instead it stretches horizontally. For
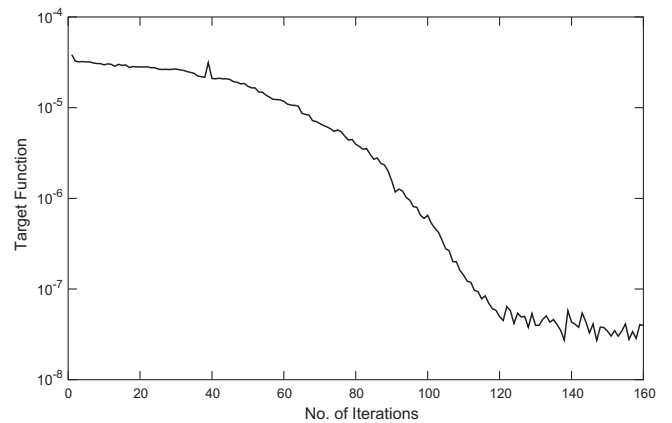
$i = 8$ the behavior is similar, but it also moves horizontally toward C. In the case for $i = 1$ the movement is mainly horizontal, and the final size is similar to C.

5.4. Simulations with a disconnected tumor region

We also simulated the case where the "data" was generated by the tumor region $C_1 \cup C_5$, and $\omega_o = C$ (see Fig. 2). The algorithm used was the one with refinement for all the 160 iterations, but with a modification in the item number 3, where we used a "while $\eta > \epsilon$" instead of the "for $i = 1 \ldots I$". The number of refinement varies between 2 and 5. In Fig. 6 we can observe how the value of the objective function decreases. Fig. 7 shows the location of ω_i (Table 1 shows its references) and the value of the temperature in the boundary Γ_u for different number of iterations. In the
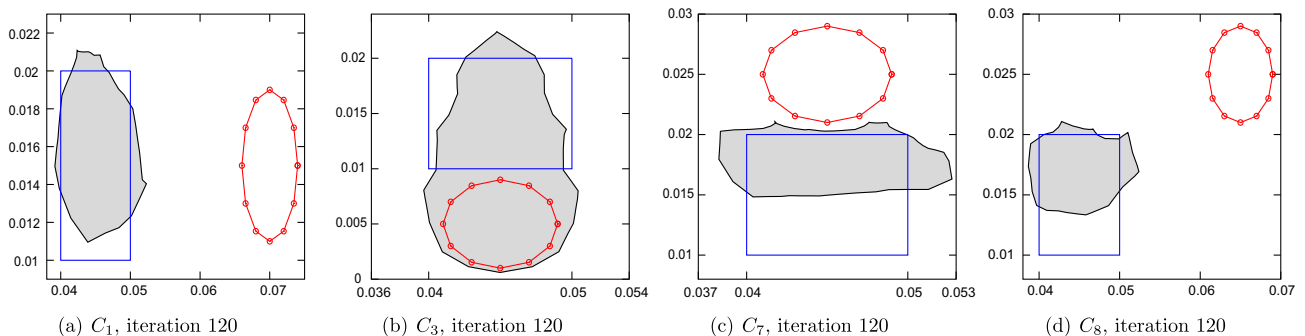

(a) C_1, iteration 120 (b) C_3, iteration 120 (c) C_7, iteration 120 (d) C_8, iteration 120

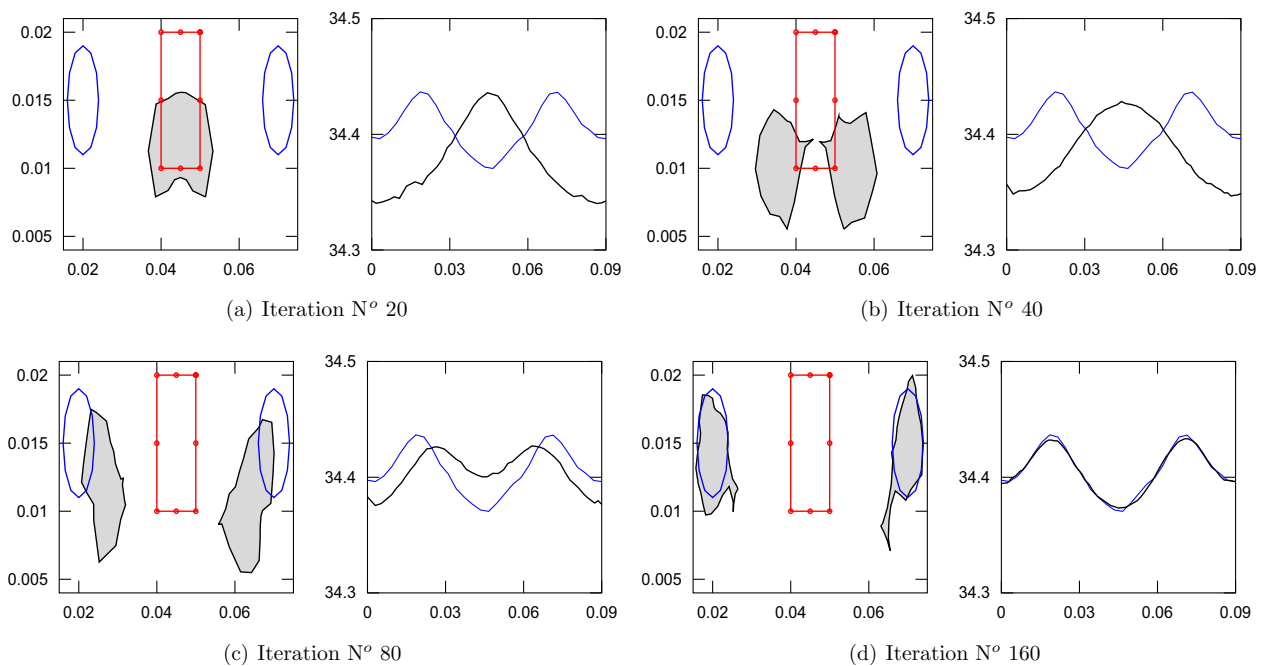**Fig. 5.** Results of the movement for different cases.

Fig. 7. Results for disconnected tumors. En each iteration we show at the left the position of the tumor and at the right the temperature in Γ_u.

iteration N° 39 the domain splits in two. The asymmetry of the two domains is generated by the non homogeneous mesh.

6. Conclusions and future work

The algorithm shows to be robust in the sense that all the seeds employed move toward the tumor location. The size and shape prediction, however, do not match with the size and shape of the tumor for most of cases. We can observe that the final value of the objective function is of the order of 10^{-7}, from which we can conclude that the information (the superficial temperature) is not enough to predict the size and shape. We have the conjecture that this method is sharp while detecting the horizontal position of the tumor, but not for the vertical position. If we consider time variation, using a thermography video as data, probably the prediction of size and shape will improve. It is important to point out that the disconnected tumors are located, even though the starting tumor is not connected.

There are many promising directions for future research. Firstly, we plan to incorporate noise into the data. Secondly, we could develop an algorithm that combines the results from simulations with different seeds. This will probably improve the prediction of the size or shape. Another method to consider for this purpose is

to have as data the skin temperature in different ambient temperatures.

References

[1] N. Salva, Problemas de Transferencia de Calor y Cambio de Fase: Resolución Analítica, Numérica, Análisis de Sensibilidad y Optimización de Forma, Ph.D. Thesis, Universidad Nacional de Rosario, Rosario, Argentina, 2012.
[2] H.W. Huang, C.L. Chan, R.B. Roemer, Analytical solutions of Pennes bio-heat transfer equation with blood vessel, J. Biomech. Eng. 116 (1994) 208.
[3] H. Pennes, Analysis of tissue and arterial blood temperature in the resting human forearm, J. Appl. Physiol. 1 (1948) 93.
[4] J.P. Agnelli, C. Padra, C.V. Turner, Shape optimization for tumor location, Comput. Math. Appl. 62 (2011) 4068.
[5] P. Clément, Approximation by finite element functions using local regularization, RAIRO (1975) 77.
[6] M. Paruch, E. Majchrzak, Identification of tumor region parameters using evolutionary algorithm and multiple reciprocity boundary element method, Eng. Appl. Artif. Intell. 20 (2007) 647.
[7] O. Pironneau, Optimal Shape Design for Elliptic Systems, Springer-Verlag, New York, 1984.
[8] R.N. Lawson, Implications of surface temperatures in a diagnosis of breast cancer, Can. Med. Assoc. J. 75 (1956) 309.
[9] R.N. Lawson, M.S. Chungtai, Breast cancer and body temperatures, Can. Med. Assoc. J. 88 (1963) 68.
[10] M. Miyakawa, J.C. Bolomey (Eds.), Non-Invasive Thermometry of Human Body, CRC Press, 1996.
[11] R. Courant, D. Hilbert, Methods of Mathematical Physics, vol. 2, Interscience Publishers Inc., 1953.